

# The BH mass of nearby QSOs: a comparison of the bulge luminosity and virial methods

M. Labita<sup>1</sup>\*, A. Treves<sup>1</sup>, R. Falomo<sup>2</sup> and M. Uslenghi<sup>3</sup>

<sup>1</sup>Department of Physics and Mathematics, University of Insubria, Via Valleggio 11, I-22100 Como, Italy

<sup>2</sup>INAF, Astronomical Observatory of Padova, Vicolo dell’Osservatorio 5, I-35122 Padova, Italy

<sup>3</sup>INAF – IASF, Via Bassini 15, I-20133 Milano, Italy

Accepted ... Received ...; in original form ...

## ABSTRACT

We report on the analysis of the photometric and spectroscopic properties of a sample of 29 low redshift ( $z < 0.6$ ) QSOs for which both *HST* WFPC2 images and ultraviolet *HST* FOS spectra are available. For each object we measure the  $R$  band absolute magnitude of the host galaxy, the CIV(1550 Å) line width and the 1350 Å continuum luminosity. From these quantities we can estimate the black hole (BH) mass through the  $M_{\text{BH}} - L_{\text{bulge}}$  relation for inactive galaxies, and from the virial method based on the kinematics of the regions emitting the broad lines. The comparison of the masses derived from the two methods yields information on the geometry of the gas emitting regions bound to the massive BH. The cumulative distribution of the line widths is consistent with that produced by matter laying in planes with inclinations uniformly distributed between  $\sim 10^\circ$  and  $\sim 50^\circ$ , which corresponds to a geometrical factor  $f \sim 1.3$ . Our results are compared with those of the literature and discussed within the unified model of AGN.

**Key words:** galaxies: active – galaxies: nuclei – quasars: general.

## 1 INTRODUCTION

Nowadays there is wide consensus that most if not all nearby early type galaxies host a supermassive black hole (SMBH) at their centers (see for a recent review Ferrarese 2006). However a direct determination of the BH mass ( $M_{\text{BH}}$ ) is possible only for a limited number of inactive galaxies in the local Universe, from dynamical methods (virial theorem) based on the observations of the kinematics of stars orbiting around the SMBH. An extension of this method to higher redshift objects is viable only for active galaxies, where  $M_{\text{BH}}$  can be derived from the dynamics of gas gravitationally bound to the SMBH: this is the usual case of regions emitting the broad emission lines (BLR).

At low redshift correlations between  $M_{\text{BH}}$  and the global properties of the host galaxies, namely the luminosity ( $L_{\text{bulge}}$ ) and the central velocity dispersion of the bulge, have been found. Locally therefore the measure of the properties of the host galaxy is an alternative method for evaluating  $M_{\text{BH}}$ .

The aim of this paper is to compare the mass determinations through the virial method and through the global parameters of the hosts of close-by quasars. For QSOs it is very difficult to measure the velocity dispersion of the stars

in the bulge, so one must rely on the  $M_{\text{BH}} - L_{\text{bulge}}$  relationship. For nearby ellipticals, there is increasing evidence that this relation has the same behavior for both inactive and active galaxies (see for example Merritt & Ferrarese 2001; McLure & Dunlop 2001, 2002; Bettoni et al. 2003), notwithstanding a substantial increase of the dispersion in the latter case, possibly due to the greater difficulty in the determination of all the parameters. Moreover, AGN hosts and inactive galaxies appear substantially the same objects, as indicated by direct morphological studies (e.g. Dunlop et al. 2003). This is consistent with a picture where the AGN phenomenon, which is linked to the gas accretion on the central BH, would be a phase characterizing the life of normal galaxies in particular during major mergers (see for example Kauffmann & Haehnelt 2000). For these reasons, in this work we start with the assumption that the correlation established for nearby galaxies is also valid for higher redshift QSOs, provided that host galaxy luminosity is corrected for galactic evolution to  $z \sim 0$ .

A second set of QSO BH mass determinations can be obtained through the virial theorem, provided that an estimate of the velocity  $v_{\text{BLR}}$  and radius  $R_{\text{BLR}}$  of the BLR is available. The BLR velocity can be derived from the FWHM of the broad emission lines if one assumes a value for the geometrical factor  $f$ , which is an unknown parameter of order unity linked to the geometry of the BLR. The measurement

\* E-mail: marzia.labita@poste.it

of  $R_{\text{BLR}}$  may require cumbersome procedures, like reverberation mapping (Ulrich et al. 1984; Blandford & McKee 1982; Peterson 2001), that uses the continuum source variability to evaluate time delays between the central emission and the BLR gas response; an alternative is to infer the BLR size from the ionizing luminosity with which it is correlated (Kaspi et al. 2000; Vestergaard 2002; Pian, Falomo & Treves 2005; Kaspi et al. 2005; Vestergaard & Peterson 2006). BH mass determinations can be then derived from a measure of the broad line widths and of the ionizing continuum intensity, once the value of the geometrical factor is fixed.

In the next section we focus on the quasar sample choice and on the data collection and analysis (2.1–2.2). In section 3 we describe the formulae used for applying the two methods of mass determination (3.1–3.2) and report on the results (3.3). This analysis constrains the value of the geometrical factor. The issue of the BLR geometry and orientation is further discussed in paragraph 3.4. In section 4 our results are compared with those of literature and discussed within the unified model of AGN.

Throughout this paper, we adopt a concordant cosmology with  $H_0 = 72 \text{ km s}^{-1} \text{ Mpc}^{-1}$ ,  $\Omega_m = 0.3$  and  $\Omega_\Lambda = 0.7$ . We have converted the results of other authors to this cosmology when adopting their relations and using their data.

## 2 THE SAMPLE AND DATA ANALYSIS

We selected<sup>1</sup> all QSOs from the Veron–Cetty & Veron (2003) catalogue, for which *HST* images and spectra are available. We further require that the images have exposure times longer than 1000 s and that spectra cover the range 1400–1700 Å (UV band). In addition we selected only objects hosted by ellipticals, so that the bulge component substantially coincides with the whole galaxy.

The resulting sample includes 29 objects at  $z < 0.6$ , 17 of which are radio loud (RLQ) and 12 are radio quiet (RQQ). The main properties of the objects are listed in Table 1. The sample is essentially uniformly distributed in redshift (see Fig. 1).

### 2.1 *HST* WFPC2 images

For 27 sources in the sample a measurement of the host galaxy magnitude and morphology is available in the literature; while for 2 objects the determination of the parameters of the host galaxy is obtained in this work: the images reduction and analysis is discussed in Appendix A and the relevant data are reported in Table 5. In order to obtain a homogeneous set of absolute magnitudes of the host galaxies, we collect from literature the values of apparent magnitude (see Table 2 for references). Since Floyd et al. (2004) didn't report the values of apparent magnitude for their objects, we derived them from absolute values and corrections they applied. For all the objects in our sample we apply color transformations to the *R* band (following Fukugita, Shimasaku & Ichikawa 1995), Galactic extinction (following

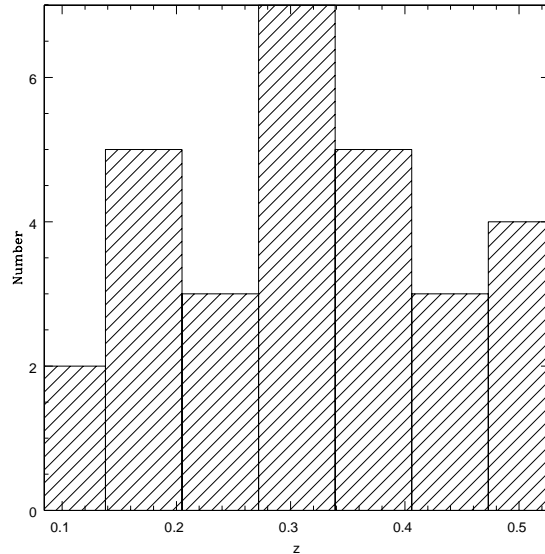


**Figure 1.** The redshift distribution of the 29 QSOs with both *HST* images and *UV* spectra.

Schlegel, Finkbeiner & Davis 1998<sup>2</sup>) and *k*-correction (following Poggianti 1997), assuming that the host galaxies are dominated by old stellar population (see Table 2). If we suppose that the host galaxies have a significant fraction of a young ( $< 1 \text{ Gyr}$ ) population, the color transformation and *k*-correction would produce magnitudes that are systematically smaller by  $\sim 0.15$  mag. Anyway, there is not strong evidence that QSO hosts in the nearby Universe ( $z \lesssim 0.5$ ) have a significative young stellar component (Nolan et al. 2001).

In Table 2 we report the *R*-band absolute magnitudes ( $M_R$ ) corrected for passive evolution (following Bressan, Chiosi & Fagotto 1994) for the 27 objects discussed above and for the 2 measured by us. Note that we have considered only QSOs hosted by elliptical galaxies; however for 2 objects (1001+291 and 1444+407) there is disagreement on the morphology of the host galaxy in literature, and our choice of an elliptical morphology follows respectively the arguments of Floyd et al. (2004) and Bahcall et al. (1997). For 19 objects, more than one estimate of the apparent magnitude was available. In these cases we have considered the mean value. The average values of the absolute *R* magnitudes (not corrected for passive evolution) are:

$$\begin{aligned} \langle M_R \rangle &= -23.47 \pm 0.81 & \text{QSOs}; \\ \langle M_R \rangle &= -23.68 \pm 0.44 & \text{RLQs}; \\ \langle M_R \rangle &= -23.18 \pm 1.10 & \text{RQQs} \end{aligned}$$

where the uncertainty is the standard deviation. The gap between the RLQ and RQQ host magnitudes is consistent with the results of other researchers (see for example Hamilton et al. 2002).

<sup>1</sup> This research has made use of the *VizieR Service*, available at <http://vizier.u-strasbg.fr/viz-bin/VizieR>.

<sup>2</sup> This research has made use of the NASA/IPAC Extragalactic Database (NED) which is operated by the Jet Propulsion Laboratory, California Institute of Technology, under contract with the National Aeronautics and Space Administration.

**Table 1.** QSOs at  $z < 0.6$  with *HST* images and spectra. These data are taken from the Veron–Cetty & Veron catalogue.

Name (1)	Alternative Name (2)	R.A. (J2000.0) (3)	Decl (J2000.0) (4)	$z$ (5)	$R_{\text{r-o}}$ (6)	$V$ (8)
0100+020	PHL 0959	01 03 12.9	+02 21 10.3	0.393	Q	16.39
0133+207	3C 047	01 36 22.4	+20 57 14.7	0.425	L	18.10
0137+012	PHL 1093	01 39 57.3	+01 31 46.2	0.272	L	17.07
0624+691	HS 0624+6907	06 30 08.6	+69 05 40.0	0.370	Q	14.20
0850+440	US 1867	08 53 34.2	+43 49 01.0	0.513	Q	16.40
0903+169	3C 215	09 06 31.9	+16 46 11.5	0.412	L	18.27
1001+291	TON 28	10 04 06.1	+28 55 19.2	0.330	Q	15.50
1136–135	PKS 1136-13	11 39 10.7	–13 50 43.6	0.554	L	16.17
1150+497	4C +49.22	11 53 22.3	+49 30 21.4	0.334	L	17.10
1202+281	PG 1202+281	12 04 42.1	+27 54 11.0	0.165	Q	15.60
1216+069	PG 1216+069	12 19 23.1	+06 38 26.8	0.331	Q	15.65
1219+755	MRK 205	12 21 45.9	+75 19 06.5	0.071	Q	15.24
1226+023	3C 273	12 29 06.7	+02 03 08.6	0.158	L	12.90
1230+097	LBQS 1230+0947	12 33 28.8	+09 31 04.9	0.415	Q	16.15
1302–102	PG 1302–102	13 05 33.0	–10 33 19.4	0.286	L	15.20
1307+085	PG 1307+085	13 09 47.0	+08 19 48.9	0.155	Q	15.10
1309+355	TON 1565	13 12 16.3	+35 14 36.7	0.184	L	15.64
1416–129	PG 1416–129	14 19 05.7	–13 10 56.5	0.129	Q	16.10
1425+267	TON 202	14 27 33.6	+26 32 52.9	0.366	L	15.68
1444+407	PG 1444+407	14 46 45.9	+40 35 05.0	0.267	Q	15.70
1512+370	PG 1512+370	15 14 39.2	+36 50 37.7	0.370	L	16.27
1545+210	3C 323.1	15 47 43.5	+20 52 16.7	0.264	L	16.70
1641+399	3C 345	16 42 58.8	+39 48 37.0	0.594	L	15.96
1704+608	3C 351	17 04 41.4	+60 44 30.5	0.371	L	15.28
1821+643	HB89 1821+643	18 22 02.8	+64 20 05.3	0.297	Q	14.10
2128–123	PKS 2128–12	21 31 35.3	–12 07 04.8	0.501	L	16.11
2135–147	PKS 2135–14	21 37 45.2	–14 32 55.8	0.200	L	15.50
2141+175	HB89 2141+175	21 43 35.5	+17 43 48.0	0.213	L	15.73
2201+315	4C +31.63	22 03 15.0	+31 45 38.3	0.295	L	15.58

## 2.2 *HST* FOS spectra

In order to have a uniform set of the spectral parameters, we performed systematically the following procedures to the available data. When more than one spectrum was available for a single object, different observations were combined into a single spectrum. Then, the continuum was fitted with a power law, removing the regions contaminated by spectral lines and by the FeII or HeII emissions. The rest-frame CIV lines of the continuum subtracted spectra are shown in Fig. 2.

In order to evaluate the virial velocity of the broad line region from *UV* spectra, we measured CIV line-widths, following i.e. Pian et al. 2005. The line widths have been measured by fitting CIV emission lines, excluding the line regions contaminated by absorption features or by the HeII(1640Å) emission. The lines have been fitted with the sum of two Gaussians with the same central wavelength, and then we derived the FWHM of the sum function. This is just a mathematical tool, and it is not related to a physical decomposition into components of different origin. We tested that, inserting a narrow ( $< 1500$  km/s) CIV component, the results remain substantially unchanged, consistently with the numerous evidences that in the *UV* spectra of QSOs the narrow line components are weak and rare (about 2 per cent occurrence rate, see Wills et al. 1993; Baskin & Laor 2005). Fig. 2 shows the adopted fits.

Since in the literature virial BH mass estimates are often based on  $H\beta$  measurements, it is interesting to compare

our FWHMs of CIV with those of  $H\beta$ . We found  $H\beta$  measurements for 25 objects of our sample in the dataset presented by Marziani et al. 2003: the average FWHM of  $H\beta$  ( $5300 \pm 2200$  km s $^{-1}$ ) is roughly consistent with that derived from our CIV measurements ( $4200 \pm 1100$  km s $^{-1}$ ). Note the larger dispersion of the  $H\beta$  measurements that is likely due to the non homogeneity of the observations from which these data were derived. The consistency between CIV and  $H\beta$  FWHMs is also supported by comparisons based on larger samples of objects (see Vestergaard et al. 2006 and references therein).

To evaluate the size of BLR through Eq. 5, we need to provide a measure of the ionizing luminosity at 1350 Å. To this aim, when a direct measure was not possible (3 cases), the value of the continuum flux ( $F_\lambda$ ) at the requested wavelength was extrapolated from the best-fitting power law. Continuum intensities were corrected for Galactic extinction, consistently with the previous section, and luminosity at 1350 Å was calculated for each object.

The relevant quantities are reported in Table 3. The uncertainty of the continuum level depends on the S/N ratio of the observations and on the intrinsic variability of the sources, giving an error of  $\sim 10$  per cent on  $F_\lambda$ . On the other hand, the uncertainty on the measured FWHM is dominated by the possible presence of absorption features and contaminating weak HeII emission nearby the CIV line. According to the shape of the CIV line, the errors on the FWHM range

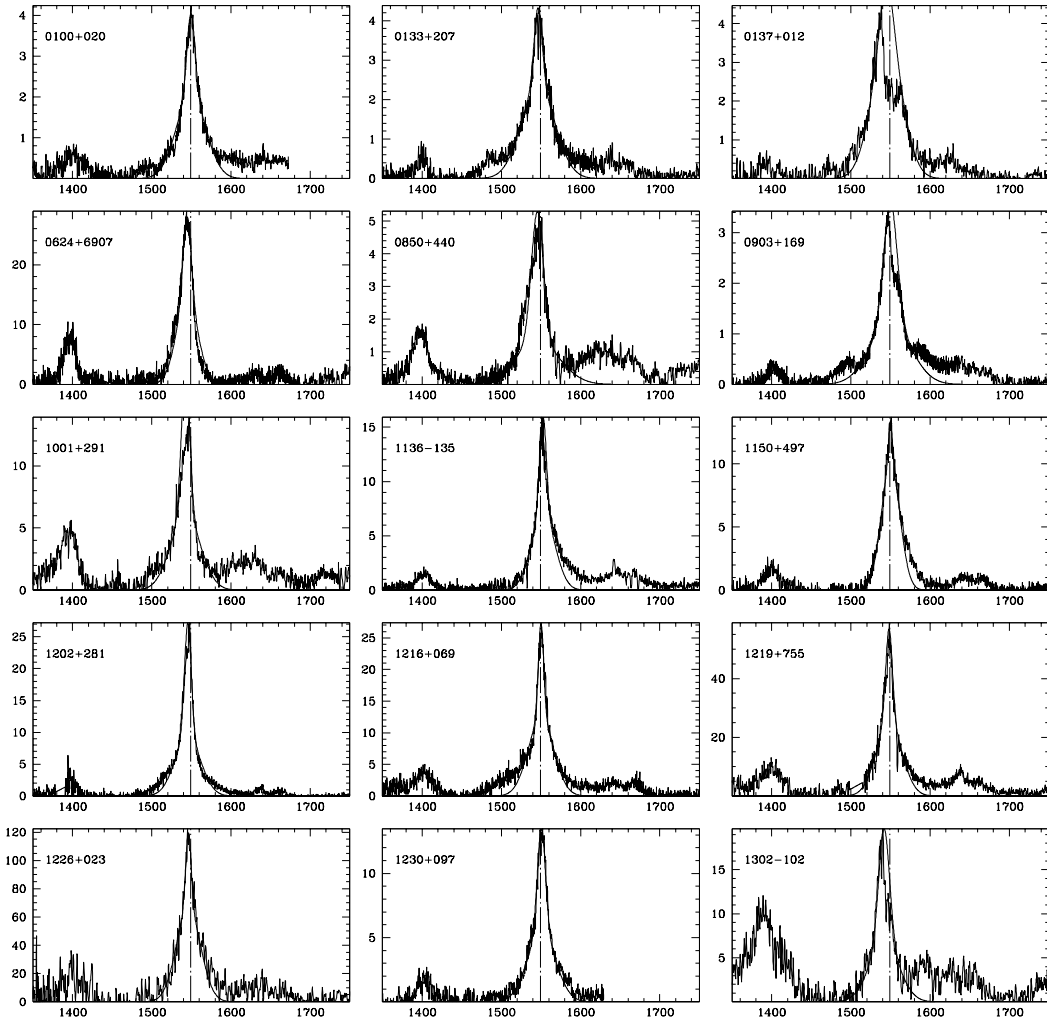


**Figure 2.** *HST* WFPC2 rest-frame continuum-subtracted spectra: CIV lines. In the  $x$ -axis,  $\lambda$  is expressed in  $\text{\AA}$ ; in the  $y$ -axis specific flux is expressed in units of  $10^{-15} \text{ erg cm}^{-2} \text{ s}^{-1} \text{\AA}^{-1}$ . The best-fitting function is also plotted for each line.

from 4 to 12 per cent, which illustrates the good quality of the data.

### 3 BH MASS DETERMINATION

#### 3.1 BH mass from the $M_{\text{BH}} - L_{\text{bulge}}$

In nearby inactive galaxies, the correlation between  $M_{\text{BH}}$  and the luminosity of the bulge component of the host has been deeply investigated (e.g. Magorrian et al. 1998; Kormendy & Gebhardt 2001; Bettoni et al. 2003). Here we use the relationship obtained by Bettoni et al. (2003), who adopted our same definition and corrections for the magnitudes. The relation corrected for the chosen cosmology is:

$$\log(M_{\text{BH}}/\text{M}_{\odot}) = -0.50M_R - 2.60 \quad (1)$$

where  $M_R$  is the absolute magnitude of the bulge component of the host galaxy. The *rms* of this fit is 0.39. This relation is close to that obtained by McLure & Dunlop (2002) for AGN host galaxies.

Thus, from the absolute magnitude of the host galaxies, corrected for passive evolution (see Table 2), we can deduce the BH masses using Eq. 1. These masses are reported in column (2) of Table 4. The mean values are:

$$\begin{aligned} \langle \log(M_{\text{BH}}/\text{M}_{\odot}) \rangle &= 8.99 \pm 0.38 & \text{QSOs;} \\ \langle \log(M_{\text{BH}}/\text{M}_{\odot}) \rangle &= 9.08 \pm 0.21 & \text{RLQs;} \\ \langle \log(M_{\text{BH}}/\text{M}_{\odot}) \rangle &= 8.86 \pm 0.52 & \text{RQQs} \end{aligned}$$

where the uncertainty is the standard deviation.

#### 3.2 BH mass from virial method

Recent studies (Gaskell 1998; Peterson & Wandel 2000; Gebhardt et al. 2000; Ferrarese et al. 2001) suggest that the black hole gravity dominates radiation pressure effects on the BLR. Assuming this and supposing that the system is in equilibrium, it is possible to use the virial theorem to evaluate the central BH mass:

$$M_{\text{BH}} = G^{-1} R_{\text{BLR}} (v_{\text{BLR}})^2 \quad (2)$$

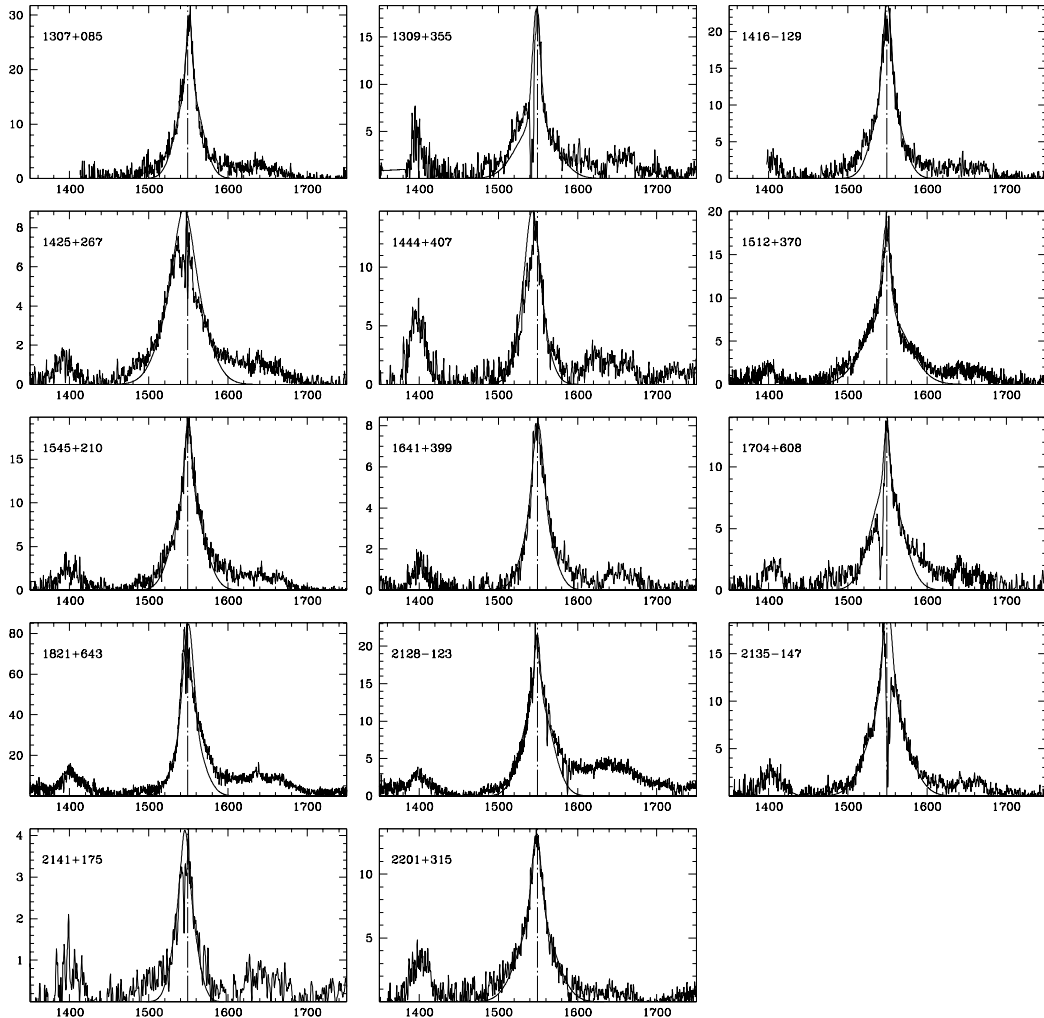


Figure 2. — continued.

where  $R_{\text{BLR}}$  is the radius of the broad line region and  $v_{\text{BLR}}$  is the gas velocity at  $R_{\text{BLR}}$ .

Under the hypothesis that the spectral line-width is caused by Doppler effect, the BLR velocity can be expressed as:

$$v_{\text{BLR}} = f \cdot \text{FWHM} \quad (3)$$

where FWHM refers to the broad emission lines produced in the BLR and is expressed in velocity units, and  $f$  is a factor related to the BLR geometry. For an isotropic field of velocities,  $f = \sqrt{3}/2$ . The issue of the value of  $f$  is discussed later on.

A relation which links  $R_{\text{BLR}}$  to the ionizing luminosity at 5100 Å was calibrated on reverberation measurements (Wandel, Peterson & Malkan 1999, Kaspi et al. 2000). Recently, this phenomenological formula has been extended outside the optical spectral range, giving expressions to derive  $R_{\text{BLR}}$  from the continuum luminosity in the UV and  $X$ -band (Vestergaard 2002; Pian et al. 2005; Kaspi et al. 2005; Vestergaard & Peterson 2006). To infer an estimate of the BLR radius, we adopt the  $R_{\text{BLR}} - L_{\lambda}(1350\text{\AA})$  relation given

in Pian et al. 2005 that was calibrated directly on reverberation measures of  $R_{\text{BLR}}$ :

$$R_{\text{BLR}} = (22.4 \pm 0.8) \left[ \frac{\lambda L_{\lambda}(1350\text{\AA})}{10^{44} \text{ erg s}^{-1}} \right]^{0.61 \pm 0.02} \text{ lt - days}, \quad (4)$$

which is consistent with that proposed by Kaspi et al. (2005), based on the study of 32 reverberation mapped AGN.

Using Eq. 3 and 4 in the virial theorem (Eq. 2), one can derive the BH mass:

$$M_{\text{BH}} = f^2 \cdot 4.4 \cdot 10^6 \left[ \frac{\lambda L_{\lambda}(1350\text{\AA})}{10^{44} \text{ erg s}^{-1}} \right]^{0.61} \left( \frac{\text{FWHM}}{1000 \text{ km s}^{-1}} \right)^2 M_{\odot} \quad (5)$$

Note that  $M_{\text{BH}}$  depends strongly on the value of the geometrical factor  $f$ .

We used the values of  $\lambda L_{\lambda}(1350\text{\AA})$  and FWHM reported in Table 3. The corresponding mass values are calculated with Eq. 5 and are given in Table 4, under the assumption of isotropy of the BLR geometry ( $f = \sqrt{3}/2$ ).

**Table 2.** Host galaxies absolute magnitudes of the 29 QSOs. NOTES – (2) 1. Hooper, Impey & Foltz 1997; 2. Hamilton, Casertano & Turnshek 2002; 3. Floyd et al. 2004; 4. Pagani, Falomo & Treves 2003; 5. Dunlop et al. 2003; 6. Boyce et al. 1998; 7. Bahcall et al. 1997; 8. Kirhakos et al. 1999; 9. this work. – (3) *R*-band mean apparent magnitudes of the host galaxies corrected for Galactic extinction. – (4) *k*-correction values following Poggianti (1997). – (5) Elliptical galaxy passive evolution correction [mag] following Bressan et al. (1994). – (6) Host galaxies absolute magnitudes corrected for passive evolution.

Name (1)	Authors (2)	$R_{ext}$ (3)	$k(R)$ (4)	$E(R)$ (5)	$M_R$ (6)
0100+020	1, 2	19.83	0.47	-0.36	-21.90
0133+207	2, 4	19.23	0.54	-0.39	-22.73
0137+012	2, 5, 6	17.42	0.28	-0.23	-23.34
0624+691	3	17.01	0.43	-0.33	-24.57
0850-144	9	19.13	0.75	-0.48	-23.44
0903+169	2, 4	19.07	0.51	-0.38	-22.81
1001+291	3	17.82	0.36	-0.29	-23.45
1136-135	9	19.12	0.87	-0.52	-23.73
1150+497	3	17.59	0.37	-0.30	-23.69
1202+281	2, 7	17.14	0.17	-0.17	-22.37
1216+069	2, 6	18.96	0.37	-0.29	-22.32
1219+755	2	15.14	0.06	-0.08	-22.57
1226+023	2, 7	15.43	0.16	-0.16	-23.93
1230+097	3	17.96	0.52	-0.38	-23.93
1302-102	2, 6, 7	17.42	0.31	-0.26	-23.44
1307+085	2, 7	17.50	0.15	-0.16	-21.85
1309+355	2, 4, 7	16.51	0.19	-0.18	-23.27
1416-129	2	17.42	0.12	-0.14	-21.44
1425+267	2, 8	18.44	0.42	-0.33	-23.08
1444+407	7	18.01	0.29	-0.24	-22.67
1512+370	2, 4	18.45	0.43	-0.33	-23.13
1545+210	2, 7	17.60	0.28	-0.24	-23.07
1641+399	8	19.31	1.01	-0.56	-23.82
1704+608	2, 6	18.00	0.43	-0.33	-23.58
1821+643	3	16.50	0.32	-0.27	-24.45
2128-123	6	19.35	0.71	-0.47	-23.14
2135-147	2, 5, 7	16.94	0.21	-0.19	-23.08
2141+175	2, 5	17.03	0.23	-0.20	-23.12
2201+315	2	16.65	0.32	-0.26	-24.30

### 3.3 Comparison of BH masses

In Fig. 3 we compare the BH masses obtained with the photometric and virial methods. As clearly shown in panel (a), the simple case of isotropic distribution of the emitting region yields inconsistent results: a systematic difference between the mass determinations obtained with the two methods is apparent ( $\langle \Delta \log(M_{\text{BH}}/\text{M}_{\odot}) \rangle = 0.36$ ).

Nevertheless, a linear relation fits well the data point and the slope of the best fit is consistent with unity ( $a = 1.1 \pm 0.2$ ). This suggests that a way of matching the two BH mass estimates is to consider the geometrical factor  $f$  as a free parameter, and to search for the value which minimizes the sum of the differences between the masses in logarithmic units from the two methods. This yields  $f = 1.3 \pm 0.1$ . Assuming this value, we report in Table 4 the corresponding virial BH masses.

In panel (b) of Fig. 3 we show the comparison of the BH masses obtained with the photometric and virial methods, adopting  $f = 1.3$ .

**Table 3.** Rest-frame spectroscopic data of the 29 analyzed objects. NOTES – (2) Rest-frame  $\text{CIV}$  FWHM values – (3) Rest-frame flux values – (4) Galactic Extinction values following Schlegel et al. 1998 – (5) Luminosity at 1350 Å.

Name (1)	FWHM [ $10^3 \frac{\text{km}}{\text{s}}$ ] (2)	$F_{\lambda}(1350\text{\AA})$ [ $10^{-15} \frac{\text{erg}}{\text{cm}^2 \text{s A}}$ ] (3)	$A_{\lambda}$ [mag] (4)	$\log(\lambda L_{\lambda})$ [ $\log \frac{\text{erg}}{\text{s}}$ ] (5)
0100+020	3.97	1.69	0.17	45.15
0133+207	4.48	1.16	0.52	45.21
0137+012	6.78	0.81	0.23	44.49
0624+691	3.58	16.72	0.80	46.35
0850+440	4.22	3.00	0.32	45.73
0903+169	4.99	0.69	0.34	44.88
1001+291	3.07	11.33	0.18	45.81
1136-135	2.94	4.19	0.40	45.99
1150+497	3.97	3.20	0.17	45.26
1202+281	2.56	2.37	0.17	44.45
1216+069	2.56	11.21	0.18	45.81
1219+755	2.94	19.71	0.37	44.74
1226+023	3.20	108.12	0.17	46.05
1230+097	3.33	5.57	0.17	45.72
1302-102	3.97	31.22	0.34	46.16
1307+085	3.33	9.20	0.28	45.03
1309+355	3.20	12.13	0.10	45.24
1416-129	3.84	3.16	0.79	44.57
1425+267	8.06	4.38	0.15	45.48
1444+407	5.12	15.91	0.11	45.71
1512+370	3.97	8.17	0.18	45.79
1545+210	4.22	5.66	0.34	45.35
1641+399	4.35	3.93	0.14	45.93
1704+608	5.12	10.92	0.19	45.91
1821+643	3.97	37.10	0.34	46.27
2128-123	4.73	7.59	0.58	46.22
2135-147	4.86	5.22	0.42	45.09
2141+175	4.22	4.54	0.90	45.27
2201+315	4.73	14.90	0.99	46.13

### 3.4 Constraining the BLR geometry

The results of the previous paragraph strongly suggest that the simplifying hypothesis of complete isotropy of the BLR, which leads to  $f = \sqrt{3}/2$ , is to be revised. Therefore we consider a scenario where there is a component of the BLR velocity field that lies on the plane of the accretion disk (see also McLure & Dunlop 2002; Jarvis & McLure 2006), in order to explore the connection between the BLR geometry and the value of the geometrical factor.

Within the unification model, we suppose that AGN are randomly oriented in space and that they are observed with the characteristics of QSO if they lie with an inclination angle  $\theta$  in a range  $\theta_{\text{MIN}} - \theta_{\text{MAX}}$ . The probability distribution to observe an object in this range is:

$$P_{\theta}(\theta) = \frac{\sin \theta}{\cos \theta_{\text{MIN}} - \cos \theta_{\text{MAX}}} \quad (6)$$

and  $P_{\theta}(\theta) = 0$  outside.

The observed FWHM of the broad emission lines is given by:

$$\text{FWHM} = 2 \left( c_1 \frac{1}{\sqrt{2}} \sin \theta + c_2 \frac{1}{\sqrt{3}} \right) v_{\text{BLR}} \quad (7)$$

where  $\sin \theta$  accounts for the projection of  $v_{\text{BLR}}$  on the line

**Table 4.** BH mass determinations. NOTES – (2)  $M_{\text{BH}}$  from the bulge luminosity (Eq. 1). – (3)  $M_{\text{BH}}$  through the virial method (Eq. 5) adopting  $f = \sqrt{3}/2$ . – (3)  $M_{\text{BH}}$  through the virial method (Eq. 5) adopting  $f = 1.3$ .

Name	$\log(M_{\text{BH}}/\text{M}_\odot)$ from $L_{\text{bulge}}$	$\log(M_{\text{BH}}/\text{M}_\odot)$ $f = \sqrt{3}/2$	$\log(M_{\text{BH}}/\text{M}_\odot)$ $f = 1.3$
(1)	(2)	(3)	(4)
0100+020	8.35	8.41	8.77
0133+207	8.76	8.55	8.91
0137+012	9.07	8.47	8.83
0624+691	9.69	9.05	9.41
0850+440	9.12	8.82	9.18
0903+169	8.80	8.44	8.80
1001+291	9.12	8.59	8.95
1136-135	9.26	8.66	9.02
1150+497	9.25	8.48	8.84
1202+281	8.58	7.60	7.96
1216+069	8.56	8.43	8.79
1219+755	8.68	7.90	8.26
1226+023	9.37	8.77	9.13
1230+097	9.36	8.60	8.96
1302-102	9.12	9.03	9.39
1307+085	8.32	8.18	8.54
1309+355	9.03	8.28	8.64
1416-129	8.12	8.03	8.39
1425+267	8.94	9.23	9.59
1444+407	8.74	8.97	9.33
1512+370	8.97	8.80	9.16
1545+210	8.94	8.59	8.95
1641+399	9.31	8.97	9.33
1704+608	9.19	9.09	9.45
1821+643	9.63	9.09	9.45
2128-123	8.97	9.22	9.58
2135-147	8.94	8.55	8.91
2141+175	8.96	8.54	8.90
2201+315	9.55	9.16	9.52

of sight and the coefficients  $\sqrt{2}$  and  $\sqrt{3}$  refer to an isotropic distribution on the plane of the accretion disk and in the 3D space respectively. The parameters  $c_1$  and  $c_2$  represent the relative fraction of FWHM due to the two velocity components. Note that, according to Eq. 3, the mean value of  $f$  can be immediately evaluated from Eq. 7:

$$\langle f \rangle = \frac{1}{2 \left( \frac{c_1}{\sqrt{2}} \langle \sin \theta \rangle + \frac{c_2}{\sqrt{3}} \right)} \quad (8)$$

where  $\langle \sin \theta \rangle$  is averaged over the probability distribution of the inclination angle (Eq. 6). With these premises, one can infer the expected cumulative FWHM distribution through Eq. (6) and (7).

In Fig. 4 we compare the distribution of the observed FWHM of the CIV lines with the expected distribution, in the cases of the two extreme assumption of complete isotropy ( $c_1 = 0$ ) and disc-like BLR geometry ( $c_2 = 0$ ).

In the isotropic case we assume that the  $v_{\text{BLR}}$  has an intrinsic Gaussian distribution with dispersion  $\sigma$ . The observed data are consistent with the expected distribution if  $\frac{\sigma}{(\text{FWHM})} = 23.4$  per cent, giving a Kolmogorov–Smirnov compatibility test with  $P(\text{KS}) \sim 99.5$  per cent (see panel (a) of Fig. 4). However, this isotropic scenario implies  $f \sim \sqrt{3}/2$  (see Eq. 8 with  $c_1 = 0$ ), and therefore it is inconsistent with

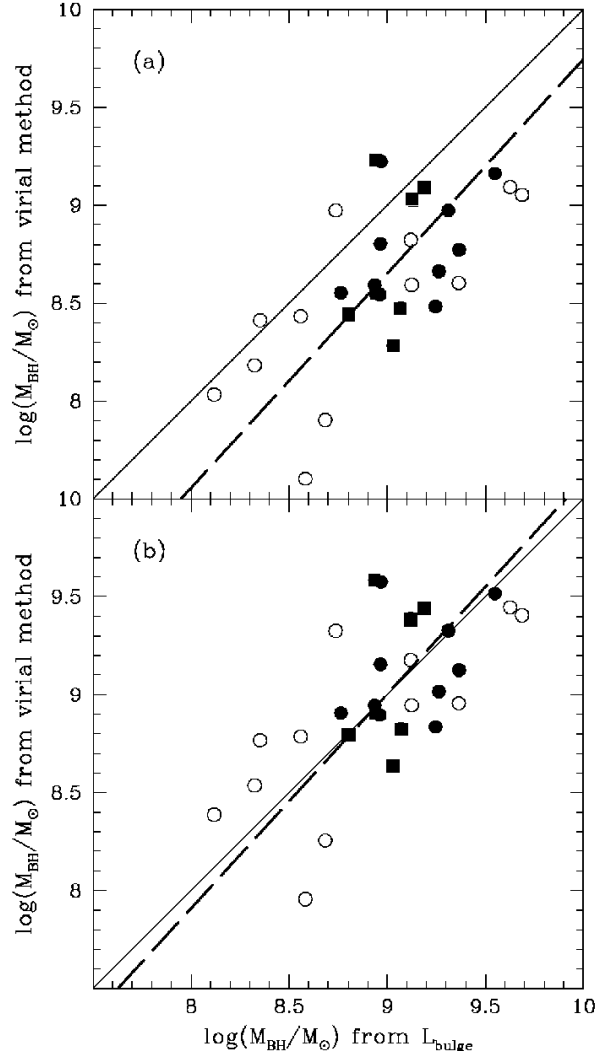


**Figure 3.** Virial BH mass determinations, adopting  $f = \sqrt{3}/2$  in panel (a) and  $f = 1.3$  in panel (b), are plotted against mass values from the  $M_{\text{BH}} - L_{\text{bulge}}$  relation. Filled (open) symbols indicate radio loud (quiet) objects. Squares highlight the objects with strong absorption features contaminating the CIV line. The solid line is the bisector; the thick dashed line is the best fit to the data.

the comparison of the BH masses through the two methods (paragraph 3.2).

In the case of disc-like geometry, we suppose that the FWHM dispersion is dominated by orientation (i.e. the intrinsic  $v_{\text{BLR}}$  dispersion is negligible). Fig. 5 shows the Kolmogorov–Smirnov probability as a function of  $\theta_{\text{MIN}}$  and  $\theta_{\text{MAX}}$ . Superimposed, we also plot the lines corresponding to fixed values of  $f$ . It is noticeable that taking  $\theta_{\text{MIN}} \sim 5^\circ - 20^\circ$  and  $\theta_{\text{MAX}} \sim 45^\circ - 50^\circ$  one has  $P(\text{KS}) > 99.5$  per cent (see also panel (b) of Fig. 4) and full consistency with the geometrical factor value ( $f \sim 1.3$ ) deduced in the previous paragraph.

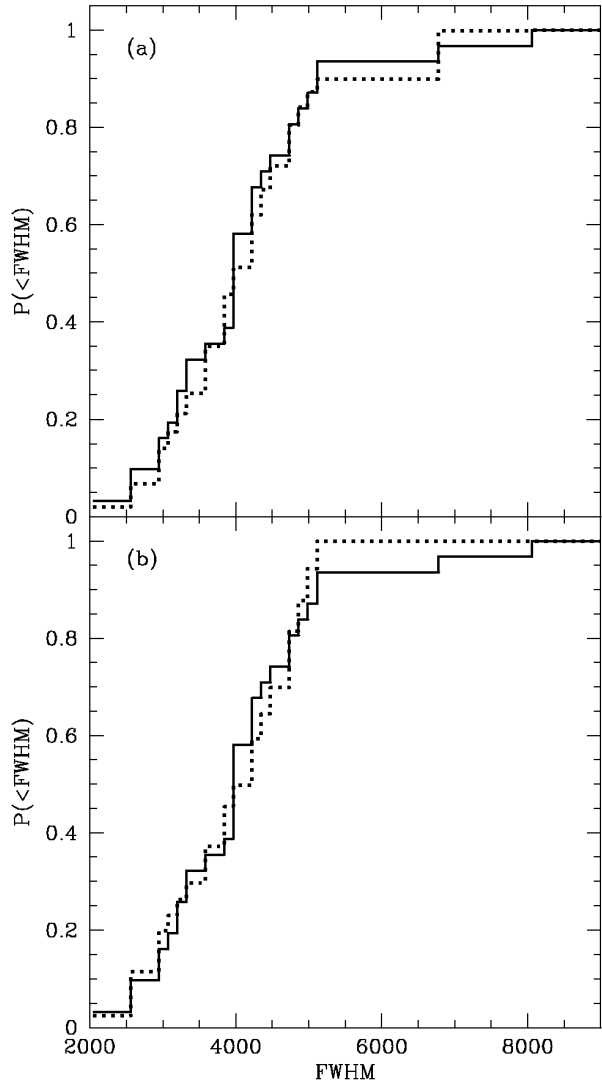


**Figure 4.** The cumulative distribution of the observed CIV FWHM (solid line) is compared in panel (a) with the Gaussian FWHM distribution which is expected under the assumption of isotropic BLR geometry (dotted line). In panel (b), the same distribution of observed FWHM (solid line) is compared with the expectations in the case of disc-like BLR geometry (dotted line), provided that inclination angles are distributed between  $12^\circ$  and  $48^\circ$  (see text for details).

#### 4 SUMMARY AND CONCLUSIONS

We have evaluated the BH masses of a sample of 29 low redshift quasars using both a photometric and a virial method. This comparison suggests the value of the geometrical factor,  $f = 1.3$ . We also found that the cumulative FWHM distribution of CIV(1550 Å) is consistent with both a disc-like BLR geometry and an isotropic velocity field, provided that in the latter case there is some distribution around the mean value of the velocity. However, the virial BH masses coincide on average with the photometric ones only in the disc picture, which strongly supports the hypothesis that the broad line region velocity field lies on the plane of the accretion disc. In this scenario, one can also put some constraints on the inclination angles of QSOs, obtaining that

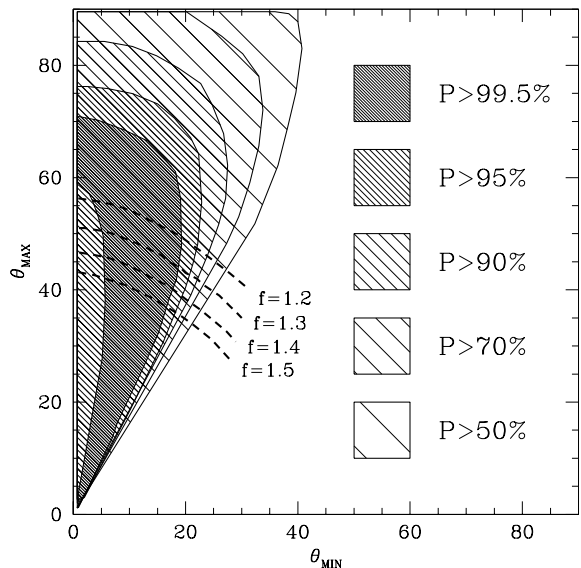


**Figure 5.** Kolmogorov-Smirnov probability values for the compatibility between the cumulative distribution of the observed CIV FWHM in our sample and the expected distribution constructed under the hypothesis of disc-like BLR geometry, in function of the minimum and maximum inclination angles. The darkest area corresponds to the highest compatibility, with  $P(KS) > 99.5$  per cent. The dashed lines indicate the locus of angles pairs which give the same geometrical factor (see text for discussion).

they are uniformly oriented between  $5^\circ - 20^\circ$  and  $45^\circ - 50^\circ$ . This result is in good agreement with the unified model of AGN (see Barthel 1989; Antonucci & Miller 1985; Antonucci 1993; Urry & Padovani 1995).

One possible caveat on this result is that we used CIV FWHM measurements instead of  $H\beta$  ones. If we adopted the  $H\beta$  FWHMs (see Section 2.2), we would obtain on average BH masses 0.2 dex larger. This would imply a value of the geometrical factor  $f \sim 1$ , which is still inconsistent with the isotropic picture.

The quasar BH masses range over two decades ( $10^8 - 10^{9.7} M_\odot$ ). Both the photometric and the virial approaches indicate that RLQ masses exceed  $10^{8.6} M_\odot$ , while RQQs are distributed in the whole mass range. RLQs have on average BH masses greater than RQQs; the difference  $\delta$  between the mean values of  $\log M_{\text{BH}}$  of the RLQ and RQQ subsamples is:

$$\delta \equiv \langle \log M_{\text{BH}}(\text{RLQ}) \rangle - \langle \log M_{\text{BH}}(\text{RQQ}) \rangle = 0.26.$$

This is in good agreement with the results obtained by Dunlop et al. (2003) and Falomo et al. (2004), who found respectively  $\delta = 0.34$  for 23 QSOs at  $\langle z \rangle = 0.2$  and  $\delta = 0.33$  for 16 QSOs at higher redshift ( $\langle z \rangle = 1.5$ ).

The general agreement between the photometric and the spectroscopic methods may be considered as an indirect indication that the  $M_{\text{BH}} - L_{\text{bulge}}$  correlation obtained locally can be extrapolated at higher redshift ( $z \sim 0.5$ ).

Our results on the BLR geometry agree well with that of the seminal paper of McLure & Dunlop (2001), who proposed that  $f = 1.5$  and obtained that a sample of 30 QSOs and 15 Seyfert I galaxies is well described by a disc-like BLR geometry, provided that it is composed of two popula-

tions with inclination angles uniformly distributed within  $0^\circ < \theta < 20^\circ$  and  $0^\circ < \theta < 46^\circ$  respectively. Our set of quasars is comparable to theirs, but the spectroscopy is of much better quality. In fact, the scatter in terms of black hole mass around the best-fitting relation of Fig. 3 ( $\sigma = 0.30$ ) is appreciably smaller than that obtained by McLure & Dunlop ( $\sigma = 0.59$ ). Our results are in good agreement also with the findings by Onken et al. (2004), who compared  $M_{\text{BH}}$  derived by the virial method with those from the stellar velocity dispersion for a sample of 16 low redshift AGN, obtaining that the geometrical factor, following our definition, is  $f \sim 1.2$ .

In conclusion, we believe that there is strong evidence that, regardless of the method used to derive BH masses, the geometrical factor results in the range  $1.0 < f < 1.3$ .

## REFERENCES

Antonucci R.R.J., 1993, A&A, 31, 473  
Antonucci R.R.J., Miller J.S., 1985, ApJ, 297, 621  
Bahcall J.N., Kirhakos S., Saxe D.H., Schneider D.P., 1997, ApJ, 479, 642  
Barthel P.D., 1989, ApJ, 336, 606  
Baskin A., Laor A., 2005, MNRAS, 356, 1029  
Bettoni D., Falomo R., Fasano G., Govoni F., 2003, A&A, 399, 869  
Blandford R.D., McKee C.F., 1982, ApJ, 255, 419  
Boroson T.A., Green R.F., 1992, ApJS, 80, 109  
Boyce P.J. et al., 1998, MNRAS, 298, 121  
Bressan A., Chiosi C., Fagotto F., 1994, ApJS, 94, 63  
Dunlop J.S., McLure R.J., Kukula M.J., Baum S.A., O'Dea C.P., Hughes D.H., 2003, MNRAS, 340, 1095  
Falomo R., Kotilainen J.K., Pagan C., Scarpa R., Treves A., 2004, ApJ, 604, 495  
Ferrarese L., 2006, in Series in High Energy Physics, Cosmology and Gravitation, 'Joint Evolution of Black Holes and Galaxies', ed. by M. Colpi, V. Gorini, F. Haardt, U. Moschella (New York – London: Taylor & Francis Group), 1  
Ferrarese L., Pogge R.W., Peterson B.M., Merritt D., Wandel A., Joseph C.L., 2001, ApJ, 555, L79  
Floyd D.J.E., Kukula M.J., Dunlop J.S., McLure R.J., Miller L., Percival W.J., Baum S.A., O'Dea C.P., 2004, MNRAS, 355, 196  
Fukugita M., Shimasaku K., Ichikawa T., 1995, PASP, 107, 945  
Gaskell C.M., 1998, ApJ, 325, 114  
Gebhardt K. et al., 2000, ApJ, 543, L5  
Hamilton T.S., Casertano S., Turnshek D.A., 2002, ApJ, 576, 61  
Hooper E.J., Impey C.D., Foltz C.B., 1997, ApJ, 480, L95  
Jarvis M.J., McLure R.J., 2006, MNRAS, preprint (astro-ph/ 0603231)  
Kaspi S., Smith P.S., Netzer H., Maoz D., Jannuzi B.T., Giveon U., 2000, ApJ, 533, 631  
Kaspi S., Maoz D., Netzer H., Peterson B.M., Vestergaard M., Jannuzi B.T., 2005, ApJ, 629, 1  
Kauffmann G., Haehnelt M., 2000, MNRAS, 311, 576  
Kirhakos S., Bahcall J.N., Schneider D.P., Kristian J., 1999, ApJ, 520, 67  
Kormendy J., Gebhardt K., 2001, 20th Texas Symp. on relativistic astrophysics, ed. J.C. Wheeler, H. Martel, AIP Conf. Proc., 586, 363  
Kotilainen J.K., Falomo R., Treves A., Uslenghi M., 2005, to appear in 'QSO hosts: evolution and environment', P.D. Barthel, D.B. Sanders, eds., 2006, Leiden University, New Astr. Rev. (astro-ph/ 0512356)  
Krist J.E., Hook R.N., 'The Tiny Tim Users manual', STScI, 1997  
Kuraszkiewicz J.K., Green P.J., Forster K., Aldcroft T.L., Evans I.N., Koratkar A., 2002, ApJS, 143, 257  
Magorrian J. et al., 1998, AJ, 115, 2285  
Marziani P., Sulentic J.W., Zamanov R., Calvani M., Dultzin-Hacyan D., Bachev R., Zwitter T., 2003, ApJS, 145, 199  
McLure R.J., Dunlop J.S., 2001, MNRAS, 327, 199  
McLure R.J., Dunlop J.S., 2002, MNRAS, 331, 795  
Merritt D., Ferrarese L., 2001, MNRAS, 320, L30  
Nolan L.A., Dunlop J.S., Kukula M.J., Hughes D.H., Boroson T., Jimenez R., 2001, MNRAS, 323, 308  
Onken C.A., Ferrarese L., Peterson B.M., Pogge R.W., Vestergaard M., Wandel A., 2004, ApJ, 615, 645  
Pagan C., Falomo R., Treves A., 2003, ApJ, 596, 830  
Peterson B.M., 2001, in Advanced Lectures on the Starburst – AGN Connection, ed. I. Artxaga, D. Kunt, R. Mijica (Singapore: World Scientific), 3  
Peterson B.M., Wandel A., 2000, ApJ, 540, L13  
Pian E., Falomo R., Treves A., 2005, MNRAS, 361, 919  
Poggianti B.M., 1997, A&AS, 122, 399  
Scarpa R., Urry C.M., Falomo R., Pesce J.E., Treves A., 2000, ApJ, 532, 740  
Schlegel D.J., Finkbeiner D.P., Davis M., 1998, ApJ, 500, 525  
Ulrich M.H. et al., 1984, MNRAS, 206, 221  
Urry C.M., Padovani P., 1995, PASP, 107, 803  
Veron-Cetty M.P., Veron P., 2003, A&A, 412, 399  
Vestergaard M., 2002, ApJ, 571, 733  
Vestergaard M., Peterson B.M., 2006, ApJ, 641, 689  
Wandel A., Peterson B.M., Malkan M.A., 1999, ApJ, 526, 579  
Wills B.J., Netzer H., Brotherton M.S., Han J.L., Wills D., Baldwin J.A., Ferland G.J., Browne I.W.A., 1993, ApJ, 410, 534

## APPENDIX A: HST IMAGING OF 2 QSO

In Table 5 we report the journal of observations for the two objects without available measurement of the host galaxy from the literature. A two-dimensional analysis has been carried out using AIDA (Astronomical Image Decomposition and Analysis, Uslenghi & Falomo 2006, in preparation; see also Kotilainen et al. 2005), a software package specifically designed to perform two dimensional model fitting of QSO images, providing simultaneous decomposition into the nuclear and host galaxy components.

PSF modelling is by far the most critical step of analysing QSO host galaxies. For HST images, the software package TinyTim (Krist & Hook 1997) can produce a PSF model that is very accurate in the inner part (up to 1–2") but it does not properly model the external fainter halo produced by the scattered light (e.g. Scarpa et al. 2000). To account for this we therefore modelled the external part by adding an exponential term to the TinyTim PSF. The parameters of these components have been evaluated by fitting the PSF model to a number of stars in the field.

For each QSO we have then applied a mask to exclude possible contamination from spurious sources, bad pixels, companions and other defects affecting the image. The background was estimated from the signal computed in a circular annulus centered on the object and its uncertainty obtained from the comparison of the values computed in annuli at different radii. The masked QSO images were finally fitted with a model including both a point source and the host galaxy assuming a de Vaucouleurs law convolved with the PSF. The results of the best fit parameters are reported in Table 5. A fit with a disc galaxy yielded significant poorer results, consistently with the high luminosity of the nucleus

**Table 5.** Journal of the unpublished *HST* WFPC2 observations and QSOs measured parameters. NOTES – (8, 9) Nucleus and host galaxy apparent magnitudes in the observation filter. – (10) Host galaxy elliptical radius. – (11) Host galaxy apparent magnitude in the  $R_{\text{Cousin}}$  band.

Name (1)	$z$ (2)	Proposal ID (3)	Obs. Date (4)	Filter (5)	$T_{\text{exp}}$ (6)	Camera (7)	$m_{\text{nuc}}$ (8)	$m_{\text{host}}$ (9)	$r_e$ (10)	$R$ (11)
0850+440	0.513	5949	07 Feb. '96	F702W	2400	WF3	16.93	18.80	1.03"	19.21
1136-135	0.554	6619	10 Jun. '97	F702W	2100	WF3	16.52	18.82	1.02"	19.23

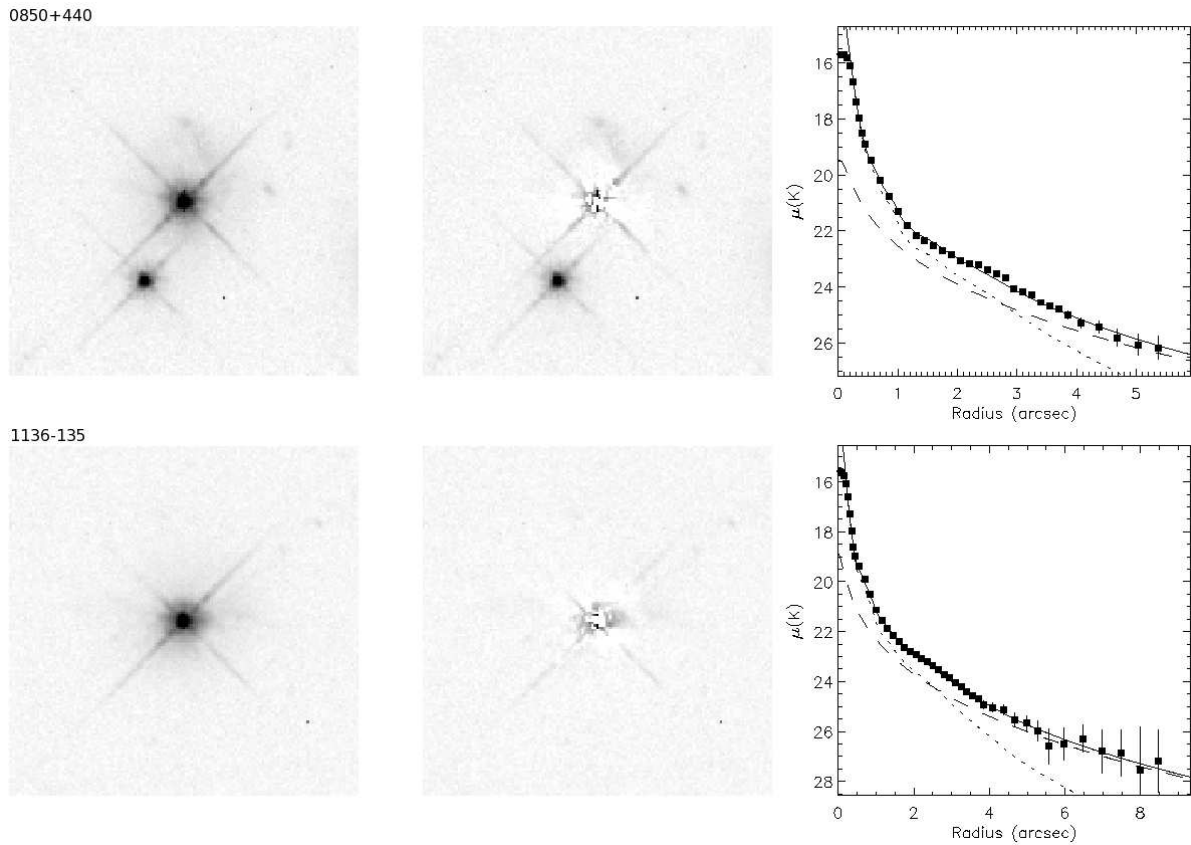


**Figure 6.** QSOs images, 2-D residuals after the PSF subtraction, and radial profiles: data points (squares), PSF (dotted lines), galaxy model (dashed lines), best-fitting convolution functions (solid lines).

(see Dunlop et al. 2003). In Fig. 6 we show the QSOs images and residuals. The radial profiles of the images, of the PSF, of the galaxy and of the best-fitting models for the 2 objects are also shown.